J. Plasma Physics (2010), *vol.* 76, *parts* 3&4, *pp.* 607–616.
doi:10.1017/S0022377809990912

Low-frequency electrostatic defect mode in doped pair-ion plasmas

I. KOURAKIS and N. S. SAINI

Centre for Plasma Physics, Department of Physics and Astronomy,
Queen's University Belfast, BT7 1NN, UK
(i.kourakis@qub.ac.uk)

(Received 15 December 2009 and accepted 18 December 2009, first published online 22 January 2010)

Abstract. The nonlinear amplitude modulation dynamics of electrostatic oscillations of massive charged defects in a three-component pair plasma is investigated, *i.e.* doped pair-ion plasmas (anticipating the injection of a massive charged component in the background, *e.g.* in fullerene experiments). Ion-acoustic oscillations in electron-positron-ion (e-p-i) plasmas are also covered, in the appropriate limit. Linear and nonlinear effects (MI, envelope modes) are discussed. The role of the temperature and density ratio between the pair species is stressed.

1. Introduction

Pair plasmas (p.p.) are characterized by the coexistence of two charged particle species which have equal masses and charges of same (absolute) value yet opposite sign. Although this formal plasma description was originally conceived to model electron-positron (*e-p*) configurations [1, 2], recent laboratory experiments pair on fullerenes (C_{60}) [3] have enabled the realization of pair-ion (C_{60}^{+}/C_{60}^{-}) plasmas, which, say, mimick the behavior of *e-p* plasmas, yet are not constrained by recombination (annihilation) processes. We shall here take the term p.p. to denote eitherpair-ion or *e-p* plasmas, yet extending its meaning to cover the existence of (a) background component(s) (*e.g.* electrons, or defects), as discussed below.

The dynamics of p.p. bears novel phenomena, which are neither trivial nor quite expected. Contrary to the traditional textbook plasma picture, where distinct frequency scales are imposed by the mass difference between electrons and ions, the two-pair species respond on the same scale. Rather surprisingly, the dynamical characteristics of pair plasmas cannot always be inferred by simply taking the limit of equal (ion and electron) masses, formally. For instance, ion-acoustic waves have no analogue in pair plasmas, where electrostatic (ES) wave dispersion obeys a Langmuir-type dispersion law [1, 2].

Although symmetric pair components were originally assumed (equal number density and temperature) in the modeling of p.p., it was soon realized that this picture may not be realistic. The remarkable features of symmetric and pure, say, p.p. may therefore be modified in the presence of either temperature fluctuations, or a charge imbalance between the pair species, due to the presence of "third" species in the background. For instance, *e-p* plasmas may also be characterized by the presence of positive ions, in addition to electrons and positrons. Electron-positron-ion (*e-p-i*) plasmas occur in astrophysics, *e.g.* in active galactic nuclei (AGN) [4]

and in pulsar magnetospheres [5], and have also been created in the laboratory [6]. On the other hand, one may anticipate the existence of a small fraction of charged massive particles in fullerene pair-ion plasma [3], either intrinsically as defects, or injected intentionally (doping) as a means of controlling plasma behavior. The above picture may be modeled by assuming (apart from the pair components) a massive background species, which may bear either positive or negative charge (the former case also formally accounts for ions in *e-p-i* plasmas). Said from the outset, another possibility, which has been suggested in the past, namely the existence of free electrons in fullerene p.p., will here be neglected.

Departing therefore from a symmetric pair-component plasma configuration, which was claimed to have been generated in the fullerene experiments mentioned above, it is virtually certain that the positive-to-negative species density and temperature ratio(s) may differ from unity (either locally or globally, *i.e.* affecting the overall charge and pressure balance). It is therefore timely and appropriate to consider the role of charged impurities (defects) in multicomponent pair plasmas.

It is obvious that multicomponent pair plasmas (as discussed above) may be characterized by two (at least) distinct frequency scales, basically delimited by the (common) pair species plasma frequency, in contrast with that of the (much heavier) background defect component. The (ES) dynamics of the pair component has generated significant interest (and controversy) in the past. Experimental investigations of low-amplitude (linear) ES oscillations suggest the existence of three distinct modes [3]. Two of these modes, namely an acoustic mode and a Langmuir-like high-frequency mode, are straightforward to predict via, *e.g.* two-fluid theory [1, 2, 7, 8]. An intermediate-frequency mode also reported [3] is viewed as a controversial topic by theoreticians, and interpretations suggested for it include soliton-trains [9], ion acoustic wave acceleration by surplus electrons [10] and Bernstein–Greene–Kruskal (BGK)-like trapped ion modes [11]. On the pair species vibration scale, nonlinear excitations predicted include solitons, either of ES [9, 12, 13] or electromagnetic (EM) [14] type, modeled by Korteweg-de Vries (KdV) (or Zakharov-Kuznetsov in 2D) theory or via the Sagdeev pseudopotential formalism. Furthermore, envelope solitons have been shown to occur on the high (pair-) frequency scale, as part of the evolution of either EM [15] or ES [7, 8] wave packets. On the other side of the scale, low-frequency oscillations of the massive background component (defects, or heavy ions) were investigated via a Krylov–Bogoliubov–Mitropolsky (KBM) perturbation technique, and were shown to be modulationally unstable at finite wavelengths [16, 17].

Our purpose here is to address the dynamics of low-frequency oscillations of the massive background component, propagating as modulated wave packets. We consider a fully ionized collisionless unmagnetized three-component plasma, consisting of two pair-species (mass $m_+ = m_- = m$, charge $q_+ = -q_- = Ze$), in addition to a background population of massive charged particles (mass $m_d = M \gg m$, charge $q_d = sZ_d e$; index d for dust, or defects); here e is the magnitude of the electron charge, and Z (Z_d) denotes the charge state of the pair (background, respectively) particle species. We choose to leave the charge sign $s = q_d/|q_d|$ arbitrary, in account of either positive or negative defects. Finally, the density and temperature ratio(s) of the pair species is (are) left arbitrary (*i.e.* not necessarily equal to unity), for generality. The role of the temperature/density asymmetry (and thus, of the stationary background species) is focused upon and will be emphasized. Pair recombination is neglected here for simplicity.

2. Model equations

We adopt a fluid model for the dynamics of electrostatic excitations of the massive background component d (for dust, or defects) in a three-component pair plasma:

$$\frac{\partial n_d}{\partial t} + \frac{\partial (n_d u_d)}{\partial x} = 0, \tag{2.1}$$

$$\frac{\partial u_d}{\partial t} + u_d \frac{\partial u_d}{\partial x} = -sZ_d \frac{e}{m_d} \frac{\partial \phi}{\partial x}, \tag{2.2}$$

$$\frac{\partial^2 \phi}{\partial x^2} = -4\pi e(sZ_d n_d - Zn_- + Zn_+), \tag{2.3}$$

where n_α ($\alpha = +, -, d$) is the number density of the respective species, u_d is the fluid velocity and ϕ is the electrostatic potential.

Given the (low-) frequency scale of interest, the pair populations can be safely assumed to be in thermal equilibrium, viz.

$$n_- = n_{-,0} \exp(Ze\phi/k_B T_-)\,, \qquad n_+ = n_{+,0} \exp(-Ze\phi/k_B T_+)\,. \tag{2.4}$$

Overall charge neutrality at equilibrium imposes $Zn_{-,0} - sZ_d n_{d,0} = Zn_{+,0}$, where the index '0' denotes the equilibrium quantities.

We shall here work with the rescaled (dimensionless) fluid equations

$$\frac{\partial n}{\partial t} + \frac{\partial (nu)}{\partial x} = 0\,, \tag{2.5}$$

$$\frac{\partial u}{\partial t} + u \frac{\partial u}{\partial x} = -s \frac{\partial \phi}{\partial x}\,, \tag{2.6}$$

$$\frac{\partial^2 \phi}{\partial x^2} \approx -s(n-1) + c_1 \phi + c_2 \phi^2 + c_3 \phi^3\,, \tag{2.7}$$

where we have expanded Poisson's equation near equilibrium. Space is scaled by the effective Debye length $\lambda_0 = (\sum_{\alpha=+,-} \frac{4\pi n_{\alpha 0} Z^2 e^2}{k_B T_\alpha})^{-1/2} \equiv (\sum_{\alpha=+,-} \lambda_{D,\alpha}^{-2})^{-1/2} \sim (\frac{n_{+0}}{T_+} + \frac{n_{-0}}{T_-})^{-1/2}$, while time is scaled by the inverse (defect) plasma frequency $\omega_{p,d}^{-1} = (4\pi n_{d0} Z_d^2 e^2/m_d)^{-1/2}$. The state variables n_d, u_d and ϕ are thus scaled as $n = n_d/n_{d0}$, $u = u_d/v_0$ and $\phi = Z_d e\phi/(k_B T_*)$, where we have defined the characteristic speed scale $v_0 \equiv (k_B T_*/m_d)^{1/2} = \omega_{p,d}\lambda_0$. The temperature scale T_* takes into account $T_\pm$ and $n_{\pm,0}$ and is determined by compatibility requirements. (Note the formal analogy with dust-acoustic waves [18].)

The coefficients entering Poisson's equation, *i.e.* (2.7) are

$$c_1 = \frac{\delta + \theta}{s(\delta - 1)}\,, \qquad c_2 = \frac{\delta - \theta^2}{2s(\delta - 1)}\,, \qquad c_3 = \frac{\delta + \theta^3}{6s(\delta - 1)}\,, \tag{2.8}$$

i.e. $c_m = [\delta - (-1)^m \theta^m]/[s(\delta - 1)m!]$ (for $m = 1, 2, 3$), all positive here. We have defined the temperature ratio θ and the dimensionless parameter δ as

$$\theta = \frac{T_-}{T_+} \qquad \delta = \frac{n_-}{n_+} = 1 + s\frac{Z_{d0} n_{d0}}{Zn_+}\,, \tag{2.9}$$

which reflects the defect concentration in the plasma. Notice that δ below (above) unity denotes negative (positive) dust/defect charge.

3. Nonlinear wave packet envelope dynamics

To model the nonlinear dynamics of the modulated amplitude of an ES wave packet in our model, we shall make use of the multiscale perturbation (or KBM) technique. The lengthy details are explained step by step in earlier works (see, *e.g.* [19]), so these need not be reproduced here. The essential information to retain for our purposes here will follow.

We consider a general stretched (slow) space and time variables scaling as $X_m = \epsilon^m x\,, \quad T_m = \epsilon^m t\,$, separating the fast carrier ($m = 0$) from the slow-amplitude (for $m \geqslant 1$) dynamics. We consider small deviations from equilibrium ($n^{(0)} = 1$ and $u^{(0)} = \phi^{(0)} = 0$), and express the state variables as $S = S^{(0)} + \sum_{m=1}^{\infty} \epsilon^m S^{(m)}$, where $\epsilon \ll 1$ is a small parameter. Here S denotes any of n, u and ϕ (all functions of $\{x, t\}$). The contribution at every order m will be a sum of (l—th) harmonics ($l = 0, 1, 2, \ldots$), viz. $S^{(m)} = \sum_{l=-m}^{m} S_l^{(m)}(X_m, T_m) \exp[il(kx - \omega t)]$. Upon substituting into (2.5–2.7), and then isolating various orders in ϵ^m and respective l—th harmonic contributions, we obtain a system for the harmonic contributions to each order.

The solution obtained for the electric potential through the long (yet perfectly straightforward) calculation is of the form

$$\phi \approx \epsilon\, \phi_1^{(1)}\, e^{i(kx-\omega t)} + \epsilon^2 \left[\phi_0^{(2)} + \phi_2^{(2)}\, e^{2i(kx-\omega t)}\right] + \cdots , \tag{3.1}$$

where the complex conjugates (c.c.) ${\phi_1^{(1)}}^*$ and ${\phi_2^{(2)}}^*$ were omitted where obvious. The expressions for n and u are analogous.

The 1st harmonic amplitudes read

$$n_1^{(1)} = s(k^2 + c_1)\phi_1^{(1)}\,, \qquad u_1^{(1)} = s\frac{\omega}{k}(k^2 + c_1)\,\phi_1^{(1)} = \frac{\omega}{k}\, n_1^{(1)}\,. \tag{3.2}$$

The dispersion relation obtained reads

$$\omega^2 = \frac{k^2}{k^2 + c_1}\,, \tag{3.3}$$

which suggests an acoustic behavior $\omega \approx k/\sqrt{c_1}$ for small k (large wavelength). We stress the dependence of the "true" phase speed $v_{ph} = v_0/\sqrt{c_1}$ and (Debye) screening length $\lambda_D = \lambda_0/\sqrt{c_1}$ (recovering dimensions for a moment) on θ and δ (via c_1).

The final outcome of the analysis, apart from a set of expressions for the various harmonics (reported in the Appendix) is a nonlinear evolution equation for the (electric potential) fundamental harmonic amplitude, say $\phi_1^{(1)} \equiv \psi(x, t)$. The nonlinear Schrödinger (NLS) equation thus obtained reads

$$i\frac{\partial \psi}{\partial T} + P\frac{\partial^2 \psi}{\partial X^2} + Q|\psi|^2\psi = 0\,, \tag{3.4}$$

where the slow independent variables here are $T = \epsilon^2 t$ and $X = \epsilon(x - v_g t)$, suggesting that the slow time-varying envelope profile moves at the group velocity $v_g = \omega'(k) = c_1\omega^3/k^3$.

The dispersion coefficient in the NLSE (3.4) is given by $P = \omega''(k)/2 = -3c_1\omega^5/(2k^4) < 0$, which varies as $P \sim k$, for small k; as a matter of fact $P \approx -3s(\delta - 1)^{3/2}/[2(\delta + \theta)^{3/2}]$ for $k \ll 1$. Note that P is negative throughout.

The nonlinearity coefficient in the NLSE (3.4) is given by a lengthy expression, here omitted, of the form $Q = Q(k; \delta, \theta)$. For small k (*i.e.* for large wavelength,

compared to the Debye length), it varies as $Q \sim 1/k$, viz.

$$Q \approx \frac{[\delta(1+2\delta)+6\delta\theta+(2+\delta)\,\theta^2]^2}{12[s(\delta-1)]^{5/2}(\delta+\theta)^{3/2}}\;\frac{1}{k}\,. \tag{3.5}$$

Note, in combination with (2.9), that the latter expression does not depend on the defect charge sign s. In fact, $P < 0 < Q$ is guaranteed for small k, ensuring stability for long wavelengths (viz. $PQ < 0$, *cf.* discussion below).

The NLSE (3.4) is well known and has been studied in detail in the past. Summarizing known results [19], we may distinguish two regimes, in terms of the product $p = PQ$ (or the ratio $r = P/Q$, say) of the coefficients P and Q.

- For negative p (or r), the wave packet is modulationally stable, and the modulated envelope may assume the form of a dark-type (black or grey) envelope soliton (*i.e.* a potential dip, propagating along with a density hole).
- For positive p (or r), the amplitude is modulationally unstable, *i.e.* a purely growing mode (imaginary frequency) develops under the effect of an external perturbation, *e.g.* due to noise or background turbulence. Modulational instability (MI) in this analytical framework is admittedly but a first-order prediction, which may presumably lead at a later stage to the wave packet's breakdown. Alternatively, an ordered state may be attained in the form of a (train of) bright envelope soliton solutions of the NLSE being formed. These bell-shaped envelope pulses are reminiscent of information pulses in nonlinear optics (*e.g.* in optical fibers), and, not surprisingly, the methodology of study is analogous.
- In either bright (for $PQ > 0$) or dark (for $PQ < 0$) soliton case, the soliton width L is related to the maximum amplitude ψ_0 as $\psi_0 L \sim (P/Q)^{1/2} = r^{1/2}$.

4. Parametric investigation

Let us first investigate from first principle the effect of the density (δ) and temperature (θ) ratios of the pair species on the linear dispersion characteristics. Recall that this is an acoustic mode, so higher frequency suggests a higher value of the phase speed $v_{ph} = \omega/k$. The analysis that follows is somehow standard, yet the consequences, say, in a potential experimental verification of our predictions are straightforward to look for.

Linear effect of the defect concentration density: pair-ion density misfit ($\delta \neq 1$). The dispersion relation of the low-frequency defect mode is depicted in Fig. 1, where we have considered both negative and positive defect charge sign cases. For negative defect charge ($\delta < 1$; see Fig. 1(a)), the frequency ω is seen to increase if lower values of δ are considered; *i.e.* with an increase in negative "dust' concentration. For positive defects ($\delta > 1$; see Fig. 1(b)), the analytical behavior is reversed (ω increases with higher δ), yet the physical interpretation is the same, namely, higher frequency with an increase in δ, and hence, in positive-defect concentration.

Linear effect of the pair-species temperature difference ($\theta \neq 1$). Considering negatively charged defects/dust, the frequency ω is seen to decrease with higher negative pair-ion temperature (increasing θ); see Fig. 2(a). The same is true for positively charged defects/dust, as obvious in Fig. 2(b).

Nonlinear characteristics. In the end of the preceding section, we have concluded that the wave packet's stability is guaranteed for small k, while MI is possible

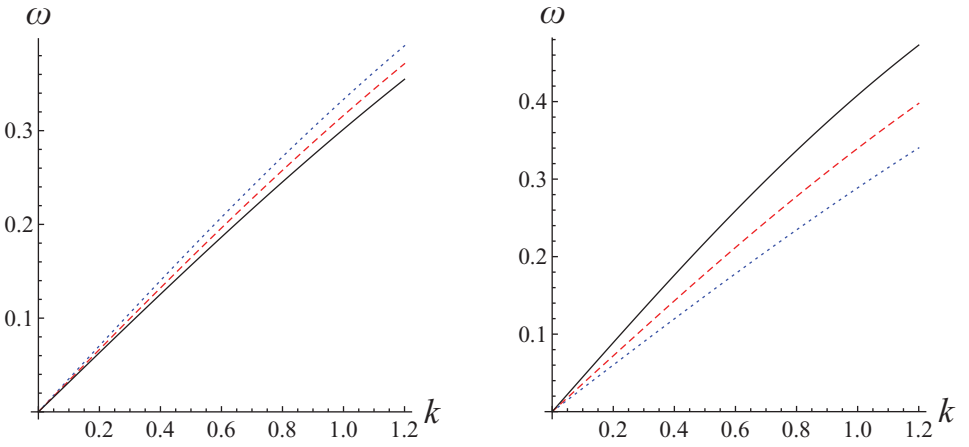

Figure 1. (Color online) Dispersion relation: the frequency ω is depicted *vs.* the wave number k, for $\theta = 1$ (equal pair species temperature). (a) (Left panel) negative defects/dust; from top to bottom, dotted curve: $\delta = 0.3$; dashed curve: $\delta = 0.4$; solid curve: $\delta = 0.5$; (b) (Right panel) positive defects/dust; from top to bottom, solid curve: $\delta = 1.5$; dashed curve: $\delta = 1.3$; dotted curve: $\delta = 1.2$.

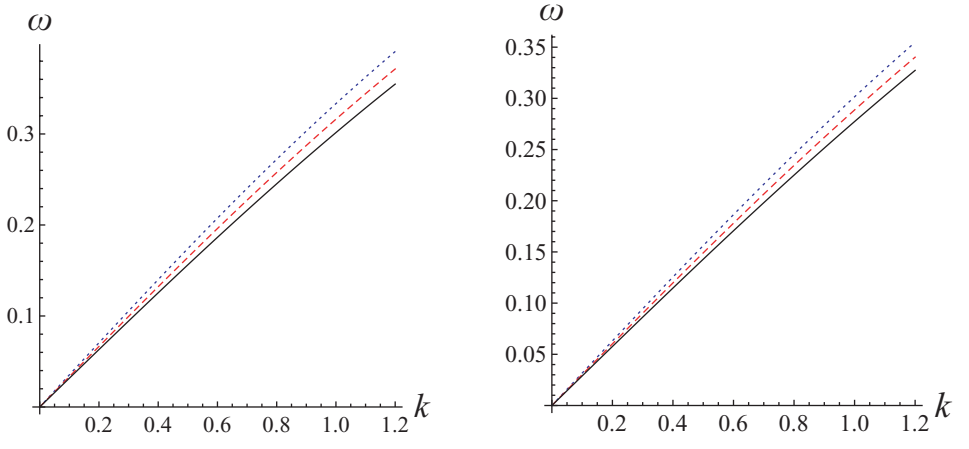

Figure 2. (Color online) Dispersion relation: the frequency ω is depicted *vs.* the wave number k, for negatively (positively) charged background defects/dust in the left panel (right panel, respectively). We have taken $\delta = 0.8$ (left panel) and $\delta = 1.2$ (right panel). From top to bottom, dotted curve: $\theta = 0.8$; dashed curve: $\theta = 1$; solid curve: $\theta = 1.2$.

for a carrier wave number value above a certain critical carrier wave number k_{cr}. The instability window (*i.e.* the range of wave number $\tilde{k}$ values for an amplitude perturbation to trigger MI extends from zero up to a threshold, which is in fact given by, say†, $\tilde{k}_0 = (2Q/P)^{1/2}|\psi_0| \sim r^{-1/2}$ (this is a nonlinear instability, so its features depend on the maximum amplitude ψ_0). The smaller the value of $\tilde{k}_0$, the more probable it is for MI to occur, and the more likely it is for bright envelope

† The amplitude perturbation wave number $\tilde{k}_0$ is here to be distinguished from the carrier wave number MI threshold k_{cr}.

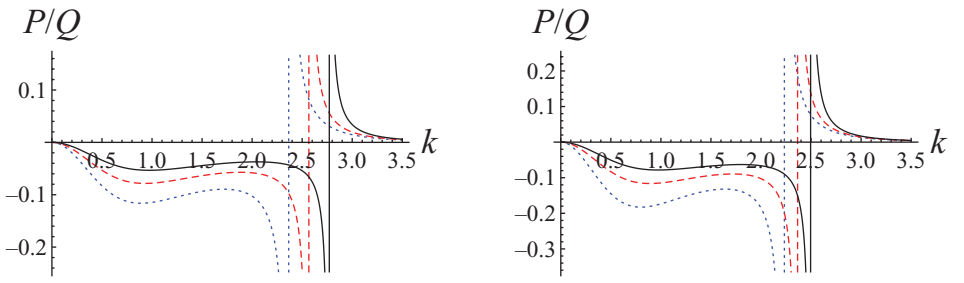

Figure 3. (Color online) Variation of the ratio P/Q *vs.* the carrier wave number k. A negatively charged background defect/dust population has been considered here. (a) (Left panel) here $\theta = 1$ (equal pair-species temperature); dotted curve: $\delta = 0.2$; dashed curve: $\delta = 0.25$; solid curve: $\delta = 0.3$. (b) (Right panel) here $\delta = 0.2$ (fixed negative defects/dust); dotted curve: $\theta = 0.8$; dashed curve: $\theta = 1$; solid curve: $\theta = 1.2$.

solitons to be formed and propagate. Furthermore, the soliton characteristics obey the relation $\psi_0 L \sim (P/Q)^{1/2} = r^{1/2}$. It is therefore appropriate to investigate the dependence of the ratio $r = P/Q$, among others, on the parameters θ and δ. Recall in the following that higher values of $r = P/Q$ imply wider envelope solitons (*i.e.* higher L for a given maximum amplitude ψ_0) in addition to a smaller threshold for MI to occur, viz.† smaller $\tilde{k}_0$.

Figure 3(a) depicts the variation of the coefficient ratio $r = P/Q$ (for negative dust) *versus* k for different values of δ and θ. For a fixed value of θ, it is noticed that the critical carrier wave number k_{cr}, at which instability sets in (*i.e.* where r changes sign), decreases as we increase the defect/dust concentration (*i.e.* with a decrease in δ). More negative defects lead to MI set in to be more likely.

In Fig. 3(b), a similar kind of behavior (increase in k_{cr}) is seen for an increase in the value of θ, for fixed $\delta = 0.2$ (negative defects/dust). The MI threshold is therefore lowered (rendering MI more probable, and bright envelope solitons more likely to occur for smaller k) by taking the negative ion component (among the pair species) to be of lower temperature (θ decreasing). The effect is reversed in the case of a positive defect background: MI is more probable (and k_{cr} is lowered) by taking the positive pair-ion to get colder (θ increasing) (or, say, the positrons, in *e-p-i* plasma). However, we have not depicted the latter situation for positive d^+ charge, since the critical value obtained numerically was unrealistically high (presumably invalidated by Landau damping).

The same analysis is iterated for a positively charged background (defects, or dust) in Fig. 4. In Fig. 4(a), keeping θ fixed (for $\theta = 1$ there), we have varied the density ratio δ; we see that the critical wave number k_{cr} decreases with an increase in the value of δ (*i.e.* an increase in the positive dust/defect concentration). Therefore, adding of more defects seems to enhance MI. In Fig. 4(b), keeping δ fixed (taking $\delta = 1.8$, *i.e.* $n_- > n_+$), we have depicted the effect of the temperature ratio θ; we observe a decrease in k_{cr} as seen for a decrease in the value of θ: MI is thus enabled (at lower k) by a colder negative (or a warmer positive) pair-ion component.

We have also investigated the behavior of the critical carrier wave number k_{cr} (where instability sets in) upon varying the value(s) of θ and/or δ. In Fig. 5, the carrier wave number threshold k_{cr} is depicted *versus* δ and θ (keeping the other parameter fixed). Our earlier conclusions made in Figs. 3 and 4 are again verified here. Note that, comparing the negative to the positive defect/dust charge case(s),

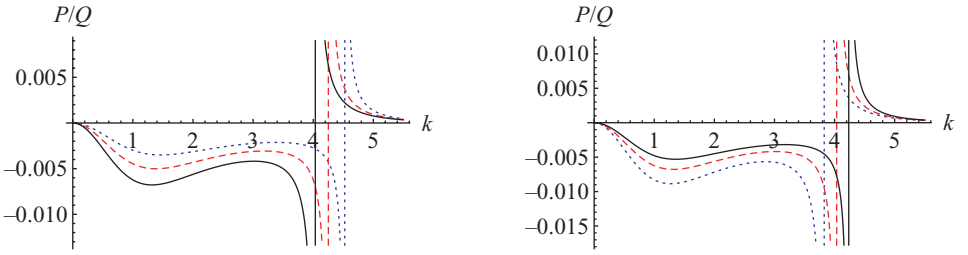

Figure 4. (Color online) Variation of the ratio P/Q *vs.* the carrier wave number k. A positively charged background defect/dust population has been considered here (formally also applying to ions in *e-p-i* plasmas). (a) (Left panel) here $\theta = 1$ (equal pair-species temperature); dotted curve: $\delta = 1.6$; dashed curve: $\delta = 1.7$; solid curve: $\delta = 1.8$. (b) (Right panel) here $\delta = 1.8$ (fixed positive defects/dust); dotted curve: $\theta = 0.8$; dashed curve: $\theta = 1$; solid curve: $\theta = 1.2$.

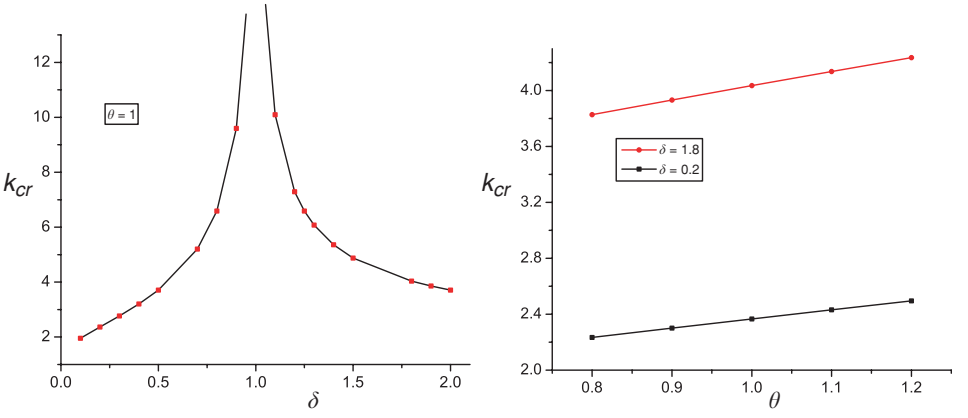

Figure 5. (Color online) Variation of k_{cr} with (a) (left panel) δ (density ratio n_-/n_+), for $\theta = 1$, and (b) (right panel) θ (temperature ratio T_-/T_+), for $\delta = 0.2$ in the lower curve, and $\delta = 1.8$ in the upper one.

we see a different analytical tendency in Fig. 4(a), which nevertheless reflects the same physical effect: more defects in the background cause a lowering of the threshold, and thus enhance modulation instability (in addition to the appearance of bright envelope solitons). On the other hand, as we see in Fig. 5(b), k_{cr} increases with an increase in θ values, *i.e.* as the negative pair component gets warmer, or the positive one gets colder.

5. Conclusions

We have investigated the linear and nonlinear dynamics of electrostatic oscillations of charged defects in three-component pair plasmas. The formulation covers either doped pair-ion plasmas, or *e-p-i* plasmas. Pair recombination was neglected. The modulational profile was studied, in particular stressing the role of a temperature and/or number density asymmetry being present between the pair species.

It may be added, for rigor, that Landau damping is inevitably overseen in this fluid model, yet could be introduced via a rigorous kinetic study. A first prediction could be inferred from analogous studies of dust acoustic waves (formally relating

defects/i^+/i^- here to dust/i^+/e^- in that case, and taking the equal mass limit). A first look in this direction suggests that damping would be controlled by the pair-plasma configuration and could be minimized [20].

Acknowledgements

The authors are happy to dedicate this article to Padma Kant Shukla, a unique colleague and a good friend, on the occasion of his 60th birthday. This work was supported by a UK EPSRC Science and Innovation award to the Centre for Plasma Physics, QUB (Grant No. EP/D06337X/1). N. S. S. gratefully acknowledges the leave granted by the authority of Guru Nanak Dev University, Amritsar, India.

Appendix. Harmonic amplitude contributions

The amplitudes corresponding to the first harmonics in order ϵ^2 are given by

$$n_1^{(2)} = s(k^2 + c_1)\phi_1^{(2)} - 2isk\frac{\partial \phi_1^{(1)}}{\partial X_1},$$

$$u_1^{(2)} = \frac{sk}{\omega}\phi_1^{(2)} - is\omega\frac{\partial \phi_1^{(1)}}{\partial X_1} \qquad \phi_1^{(2)} = i\tilde{A}\frac{\partial \phi_1^{(1)}}{\partial X_1}, \tag{A 1}$$

where the choice of $\tilde{A}$ is arbitrary and we shall take it equal to zero.

For $m = 2$ and $l = 2$, the evolution equations provide the amplitudes of the second-order harmonics as

$$n_2^{(2)} = C_1^{(22)}{\phi_1^{(1)}}^2, \quad u_2^{(2)} = C_2^{(22)}{\phi_1^{(1)}}^2 \quad \text{and} \quad \phi_2^{(2)} = C_3^{(22)}{\phi_1^{(1)}}^2, \tag{A 2}$$

$$C_1^{(22)} = sc_2 + s(4k^2 + c_1)C_3^{(22)}, \quad C_2^{(22)} = \frac{\omega}{k}\big(C_1^{(22)} - (k^2 + c_1)^2\big), \quad \text{and}$$

$$C_3^{(22)} = -\frac{c_2}{3k^2} + \frac{s(k^2 + c_1)^2}{2k^2}. \tag{A 3}$$

Combining the equations obtained for $(m = 2, l = 0)$ and $(m = 3, l = 0)$,

$$n_0^{(2)} = C_1^{(20)}\big|\phi_1^{(1)}\big|^2, \quad u_0^{(2)} = C_2^{(20)}\big|\phi_1^{(1)}\big|^2 \quad \text{and} \quad \phi_0^{(2)} = C_3^{(20)}\big|\phi_1^{(1)}\big|^2, \tag{A 4}$$

$$C_1^{(20)} = s\big(c_1 C_3^{(20)} + 2c_2\big), \quad C_2^{(20)} = -\frac{2\omega}{k}(k^2 + c_1)^2 + v_g C_1^{(20)} \quad \text{and}$$

$$C_3^{(20)} = \frac{2c_2 v_g^2 - s(k^2 + 3c_1)}{1 - c_1 v_g^2}. \tag{A 5}$$

To third order in ϵ, the reduced equations for $l = 1$ yield an explicit compatibility condition, which reduces to the NLSE (3.4). The nonlinearity coefficient Q is

$$Q = \frac{\omega^3}{k^2}\left[c_2\big(C_3^{(20)} + C_3^{(22)}\big) + \frac{3}{2}c_3\right] - \frac{\omega}{2}\big(C_1^{(20)} + C_1^{(22)}\big) - k\big(C_2^{(22)} + C_2^{(20)}\big). \tag{A 6}$$

References

[1] Iwamoto, N. 1993 Collective modes in nonrelativistic electron-positron plasmas. *Phys. Rev.* E **47**, 604–611.

[2] Zank, G. P. and Greaves, R. G. 1995 Linear and nonlinear modes in nonrelativistic electron-positron plasmas. *Phys. Rev.* E **51**, 6079–6090.

[3] Oohara, W. and Hatakeyama, R. 2003 Pair-ion plasma generation using fullerenes. *Phys. Rev. Lett.* **91**, 205005/1–4; Oohara, W., Date, D. and Hatakeyama, R. 2005 Electrostatic waves in a paired fullerene-ion plasma. *Phys. Rev. Lett.* **95**, 175003/1–4; Hatakeyama, R. and Oohara, W. 2005 Properties of pair-ion plasmas using fullerenes. *Phys. Scr.* **116**, 101–104.

[4] Miller, H. R. and Witta, P. J. 1987 Active Galactic Nuclei. Berlin, Germany: Springer-Verlag, p. 202.

[5] Michel, F. C. 1982 Theory of pulsar magnetospheres. *Rev. Mod. Phys.* **54**, 1–66.

[6] Greaves, R. G. and Surko, C. M. 1995 An electron-positron beam-plasma experiment. *Phys. Rev. Lett.* **75**, 3846; Berezhiani, V. I., Tskhakaya, D. D. and Shukla, P. K. 1992 Pair production in a strong wake field driven by an intense short laser pulse. *Phys. Rev.* A **46**, 6608; Surko, C. M., Levelhal, M., Crane, W. S., Passne, A. and Wysocki, F. 1986 Use of positrons to study transport in tokamak plasmas. *Rev. Sci. Instrum* **57**, 1862; Surko, C. M. and Murphay, T. 1990 Use of the positron as a plasma particle. *Phys. Fluid* B **2**, 1372–1375.

[7] Kourakis, I., Esfandyari-Kalejahi, A., Mehdipoor, M. and Shukla, P. K. 2006 Modulated electrostatic modes in pair plasmas: modulational stability profile and envelope excitations. *Phys. Plasmas* **13**, 052117; Esfandyari-Kalejahi, A., Kourakis, I. and Shukla, P. K. 2006 Oblique modulation of electrostatic modes and envelope excitations in pair-ion and electron-positron plasmas. *Phys. Plasmas* **13**, 122310/1–9.

[8] Esfandyari-Kalejahi, A., Kourakis, I., Mehdipoor, M. and Shukla, P. K. 2006 Electrostatic mode envelope excitations in e-p-i plasmas application in warm pair ion plasmas with a small fraction of stationary ions. *J. Phys. A: Math. Gen.* **39**, 13817–13830.

[9] Verheest, F. 2006 Existence of bulk acoustic modes in pair plasmas. *Phys. Plasmas* **13**, 082301.

[10] Saleem, H., Vranjes, J. and Poedts, S. 2006 On some properties of linear and nonlinear waves in pair-ion plasmas. *Phys. Lett.* A **350**, 375–379.

[11] Schamel, H. and Luque, A. 2005 Kinetic theory of periodic hole and double layer equilibria in pair plasmas. *New J. Phys.* **7**, 69/1–9; Schamel, H. 2008 Ion holes in dusty pair plasmas. *J. Plasma Phys.* **74**, 725–731.

[12] Lazarus, I. J., Bharuthram, R. and Hellberg, M. A. 2008 Modified Korteweg-de Vries-Zakharov-Kuznetsov solitons in symmetric two-temperature electron-positron plasmas. *J. Plasma Phys.* **74**, 519–529.

[13] Kourakis, I., Moslem, W. M., Abdelsalam, U. M., Sabry, R. and Shukla, P. K. 2009 Nonlinear dynamics of rotating multi-component pair plasmas and e-p-i plasmas. *Plasma and Fusion Research* **4**, 018/1–11.

[14] Verheest, F. and Cattaert, T. 2005 Oblique propagation of large amplitude electromagnetic solitons in pair plasmas. *Phys. Plasmas* **12**, 032304.

[15] Kourakis, I., Verheest, F. and Cramer, N. 2007 Nonlinear perpendicular propagation of ordinary mode electromagnetic wave packets in pair-ion and electron-positron-ion plasmas. *Phys. Plasmas* **14**, 022306/1–10.

[16] Salahuddin, M., Saleem, H. and Saddiq, M. 2002 Ion-acoustic envelope solitons in electron-positron-ion plasmas. *Phys. Rev.* E **66**, 036407/1–4.

[17] Jehan, N., Salahuddin, M., Saleem, H. and Mirza, A. M. 2008 Modulation instability of low-frequency electrostatic ion waves in magnetized electron-positron-ion plasma. *Phys. Plasmas* **15**, 092301.

[18] Kourakis, I. and Shukla, P. K. 2004 Oblique amplitude modulation of dust-acoustic plasma waves. *Phys. Scripta* **69**, 316–327.

[19] Kourakis, I. and Shukla, P. K. 2005 Exact theory for localized envelope modulated electrostatic wavepackets in space and dusty plasmas. *Nonlin. Proc. Geophys.* **12**, 407–423.

[20] Lee, M.-J. 2007 Landau damping of dust acoustic waves in a Lorentzian plasma. *Phys. Plasmas* **14**, 032112.